Nonequilibrium Molecular Dynamics Simulations of Steady-State Heat and Mass Transport in Distillation

Signe Kjelstrup* and Bjørn Hafskjold

Department of Physical Chemistry, Norwegian University of Science and Technology, N-7034 Trondheim, Norway

Coupled transport phenomena across a gas/liquid interface, relevant for distillation, were studied by nonequilibrium molecular dynamics simulations. The simulations were set in the context of bulk irreversible thermodynamics. It was then shown that mole fraction profiles in the liquid phase and the gas phase of ideal isotope mixtures are linear. For nonideal mixtures, Fick's law cannot be applied in the interface region, because the activity coefficients change dramatically across the interface. Fourier's law has a constant heat conductivity for both types of liquid mixtures but not for gas mixtures. The coupling between heat and mass transfer becomes negligible for distillation in the special case of ideal mixtures with constant molal overflow. In all other cases, the heat of transfer contributes significantly to the heat flux and causes deviations from Fourier's law in the gas phase. This all means that coupled flux equations are needed to describe distillation and that the properties of the surface are important for a description of the heat and mass fluxes involved. The value of the heat of transfer has a bearing on the calculation of the number of theoretical stages in the column. When considered as a function of distance from the surface, the local entropy production rate has a peak or a shoulder (depending on the conditions) slightly into the vapor. The entropy production rate in the liquid cannot be neglected compared to that of the gas. The second law efficiency of distillation was quantified from this knowledge.

Introduction

The standard process simulation of distillation columns uses the equilibrium stage model. This type of simulation does not yield the accuracy required for modern column design and operation when applied to distillation of multicomponent mixtures and to mixtures with a chemical reaction (Taylor and Lucia, 1995). A separation process is by nature a nonequilibrium process, so nonequilibrium models for heat and mass transfer might well give a better description of the separation. The purpose of this work is to contribute to the development of nonequilibrium modeling of heat and mass transfer in distillation.

We shall use the theory of nonequilibrium thermodynamics, as given by de Groot and Mazur (1961) and Førland et al. (1988), to formulate the necessary and sufficient fluxes and forces for transport taking place in the column. The advantage of this theory is that the variables being used also define the entropy production rate. The description is therefore suitable for optimization procedures based on the second law of thermodynamics. An optimization criterion, the principle of equipartition of forces, was already developed on these grounds (Sauar et al., 1996) and applied to distillation (Kjelstrup Ratkje et al., 1995; Sauar et al., 1995). Nonequilibrium thermodynamic theory contains the main transport coefficients for heat and mass flux (thermal conductivity and diffusion coefficients), plus the so-called cross coefficients, relating the heat flux to the concentration gradient and the mass flux to the temperature gradient. Since the cross terms couple the variables, some of which are experimentally very difficult to obtain, it is a central issue to know when they can be neglected and when they become significant. In other words, when can we safely use Fick's and Fourier's laws, and when do they fail? This is one question of practical importance which can be addressed in the context of nonequilibrium thermodynamics.

In the modeling of heat and mass transfer in distillation, the two phases have very different transport properties, and the liquid/vapor interface adds to the complexity of the system. It is necessary to relate compositions and temperatures on each side of the interface, and the role of the interface is crucial in this respect. Can we, for instance, assume continuity in the temperature across the interface? Theoretical results by Bedeaux et al. (1990, 1992) show that this may not be so on a macroscopic length scale. These authors discussed how interfaces, which have very different properties from those of the adjacent bulk phases, affect the boundary conditions for the bulk phases. Knowledge of this is therefore important for a dynamic description.

The entropy production rate is defined as the product sum of all fluxes and their conjugate forces in the system. Each flux is a linear combination of all independent forces. The entropy production rate for separation of two components across a liquid/vapor interface can be written as (see, e.g., Kjelstrup Ratkje and Hafskjold, 1996)

$$\theta = -J_q \frac{\nabla T}{T^2} - J_{\mathrm{h}}^{\mathrm{r}} \frac{\nabla_T \mu_{\mathrm{h}}}{T} \tag{1}$$

The measurable heat flux, J_q, is given in W m^{-2}, and the molar flux, $J_{\mathrm{h}}^{\mathrm{r}}$, is the flux (in mol m^{-2} s^{-1}) of the heavy component, h, relative to the light component, l:

$$J_{\mathrm{h}}^{\mathrm{r}} = J_{\mathrm{h}} - \frac{x_{\mathrm{h}}}{x_{\mathrm{l}}} J_{\mathrm{l}} \tag{2}$$

where x_{k} is the mole fraction of component k (k = h, l).

* To whom correspondence should be addressed. Also, the author changed her last name from Ratkje. Telephone: 47-7359-4179. Telefax: 47-7359-1676. Email: ratkje@kjemi.unit.no.

S0888-5885(96)00199-6 CCC: $12.00

This flux is defined to give Stefan diffusion (Taylor and Krishna, 1993). For a direct physical interpretation of the relative molar flux, also see eq 6. Here J_h and J_l are given with the surface as the frame of reference. The relative flux, J_h^r, gives a more convenient chemical force as used before (Kjelstrup Ratkje et al., 1995). There is a certain degree of freedom in the choice of fluxes and forces. The entropy production rate is, of course, invariant to the choice. With the fluxes given above, the thermal force is $\nabla(1/T)$, where T is the temperature, and the chemical force is $-\nabla_T \mu_h/T$, where μ_h is the chemical potential of h. Subscript T means that the temperature derivative of the chemical potential gradient is not taken. It follows from eq 1 that the number of independent thermodynamic forces is two. Although the fluxes and forces are vectors, we consider here only the contributions normal to the interface. We choose this normal to be the x direction, which gives $\nabla = \partial/\partial x$.

The fluxes of heat and mass in the column are linearly related to these forces by

$$J_q = -l_{qq}\frac{\nabla T}{T^2} - l_{qh}\frac{\nabla_T \mu_h}{T} \tag{3}$$

$$J_h^r = -l_{hq}\frac{\nabla T}{T^2} - l_{hh}\frac{\nabla T \mu_h}{T} \tag{4}$$

The phenomenological coefficients (the l coefficients) are properties of the system; i.e., their values depend on the system's local intensive thermodynamic variables. Onsager's reciprocity relation ($l_{hq} = l_{qh}$) was confirmed for a supercritical state by nonequilibrium molecular dynamics simulations by Hafskjold and Kjelstrup Ratkje (1995) for much larger gradients than found in a distillation column, and we shall assume validity also in the present case. When the coupling coefficients l_{hq} and l_{qh} can be neglected, or one of the fluxes is zero, eq 3 and 4 can be recast into the form of Fourier's and Fick's laws (see below).

Standard engineering texts uses the assumption of constant molal overflow to find the number of theoretical stages in a McCabe−Thiele diagram (see any textbook in chemical engineering, e.g., Lydersen, 1983). This assumption, which means that the number of moles of liquid entering one stage equals the number of moles of liquid leaving the same stage, implies operating lines with constant slopes. In eq 2, constant molal overflow means $J_h = -J_l$ (equimolar counterdiffusion). The enthalpies of vaporization of the components are taken to be almost the same under constant molal overflow (Lydersen, 1983). In the general situation, the enthalpies are different, and the operating line is bending. Nonequilibrium thermodynamics does not use the assumption of constant molal overflow *a priori*, and the possible bending of the operating line is a consequence of a significant coupling term in eqs 3 and 4. Nonequilibrium thermodynamics therefore gives a more general description of distillation.

The minimum energy needed to separate an isothermal mixture is the Gibbs energy of separation, ΔG, representing a reversible process. The energy needed in excess of the Gibbs energy is the local entropy production rate per unit volume, θ, times the absolute temperature, T, integrated over the column volume, V, and time, t (Kjelstrup Ratkje et al., 1995). The total work needed for the separation is then

$$W = \Delta G + \int_t \int_V T\theta \, dV \, dt \tag{5}$$

For reversible conditions, θ is zero. This corresponds to the condition of zero thermodynamic loss (Dhole and Linnhoff, 1993). This is a situation of no practical interest, because such processes are infinitely slow. It has long been known that close to global equilibrium, minimum entropy production occurs at steady states (Prigogine, 1947). In order to obtain a more useful result, Tondeur and Kvaalen (1987) proposed that the distribution of the entropy production rate over the process equipment should be uniform. We have shown that the entropy production rate will be minimum, for a given demand on the output, when the *forces* of eqs 3 and 4 are equipartitioned over the process equipment (Kjelstrup Ratkje et al., 1995; Sauar et al., 1996). While special knowledge of the phenomenological coefficients is not necessary for the direct application of the principle of equipartition of forces, such knowledge is useful in finding potential regions of reduction of the entropy production. In their attempt to numerically estimate the entropy production of a distillation column, Kjelstrup Ratkje et al. (1995) used the assumption of negligible entropy production in the liquid phase as well as on the surface. Other assumptions, which are not good for actual columns, were constant phenomenological coefficients and area for transfer on each stage. In the present work, we do not need such assumptions, as we calculate the entropy production rate directly from molecular properties. The results obtained can therefore be used to discuss the previously used assumptions.

Information about fluxes and forces in eqs 3 and 4 helps us to quantify the energy efficiency of the column through eq 5. Through the variables and coefficients of eqs 3 and 4, we know which processes are rate limiting, and from eq 5, we then know where the energy is required for separation. In this way, eqs 3−5 are important for column design and operation: They give the second law efficiency of the column (through eq 5) and enable the application of the principle of equipartition of forces.

It is very laborious to measure the transport coefficients for a gas/liquid interface, the forces, the fluxes, and thus the entropy production rate. This makes nonequilibrium molecular dynamics simulations (NEMD) an attractive tool for the study of such systems. In a recent review (Kjelstrup Ratkje and Hafskjold, 1996), we analyzed some natural and technical processes that are characterized by transport of heat and mass, in terms of NEMD; the basic finding was that the molecules of the systems distribute in a stationary-state temperature gradient so as to conduct heat (or mass) in the most effective way. The systems reported included transports of heat and mass both in a binary, homogeneous mixture and in a one-component system undergoing a liquid−vapor phase transition (Ikeshoji and Hafskjold, 1994; Hafskjold and Ikeshoji, 1996).

In this article, we continue the work on nonequilibrium thermodynamics and NEMD which are relevant for distillation. We want to study heat and mass transfer across the liquid/vapor interface and, in particular, spatial variations in entropy production rate, fluxes, and forces. The following questions are of interest: What are typical variations in temperature and composition across an interface, given a temperature gradient across the system? In Fick's law of diffusion, the concentration gradient is the driving force of transport. Is this applicable to the system? What

are the conditions for application of Fourier's law? The coupling coefficients are relatively small in bulk materials (Kincaid et al., 1992; Kincaid and Hafskjold, 1994). We shall see that the term containing the coupling coefficient (*i.e.*, the heat of transfer) cannot be neglected in the expression for heat fluxes in distillation-like phenomena. How do the entropy production rate and the conjugate fluxes and forces vary across the interface in this situation? What are the major contributions to the entropy production? Can the results support the assumptions in the numerical analysis of distillation columns of Sauar and co-workers (1995, 1996)? Which practical consequences can be seen from the results? Is the steady-state situation compatible with uniform distribution of the entropy production (Tondeur and Kvaalen, 1987)?

This paper starts with a summary of some concepts from nonequilibrium thermodynamics. We continue with a short description of the NEMD method before we give the results of the simulations. Variations of intensive variables across the interface, fluxes, and forces for separation of isotope (ideal) mixtures and nonideal mixtures are reported. NEMD simulation data of these systems also offer the possibility of extracting phenomenological coefficients for the bulk and for the surface as such, and we shall to some extent discuss the diffusion coefficient and the thermal conductivity. The molecular interpretation of their values, however, is outside the topic of the present paper and will be given later. Finally, we discuss the local entropy production and the application of the results to analyses of distillation.

Heat and Mass Transports in a Distillation Column

In a distillation column, gas is in close contact with liquid, and the main question we address here is how the interface influences the transport processes. We consider a planar interface with infinitely large reservoirs of matter and heat both in the gas and liquid phases. The transport path is chosen from a point in the bulk gas to a point in the bulk liquid, and we describe the exchange of components h (heavy) and l (light) and of heat, between the gas and liquid. The driving forces are a temperature gradient and a chemical potential gradient, as in eqs 3 and 4. Component l, the component with the lowest boiling point, is enriched at the top of the distillation column.

The relative molar flux of component h is also related to its velocity by

$$J_{\mathrm{h}}^{\mathrm{r}} = c_{\mathrm{h}}(v_{\mathrm{h}} - v_{\mathrm{l}}) \tag{6}$$

where v_k is the velocity of component k (k = h, l) relative to the interface (dimension m s^{-1}) and c_h is the molar concentration of component h (mol m^{-3}). There is no separation when $J_h^r = 0$, which makes this flux a measure of practical interest.

The heat of transfer, q^*, is defined by the coefficient ratio l_{qh}/l_{hq} and by

$$J_q = -\lambda\nabla T + q^* J_{\mathrm{h}}^{\mathrm{r}} \tag{7}$$

The heat of transfer refers to the relative flux, J_h^r, according to this equation. The thermal conductivity is from eqs 3, 4, and 7:

$$\lambda = \frac{1}{T^2}\left(l_{qq} - \frac{l_{\mathrm{h}q}l_{q\mathrm{h}}}{l_{\mathrm{hh}}}\right) \tag{8}$$

Fourier's law for the nonuniform mixture is obtained when the mass flux is zero:

$$(J_q)_{J_{\mathrm{h}}^{\mathrm{r}}=0} = -\lambda\nabla T \tag{9}$$

We shall say here that Fourier's law applies when the thermal conductivity of eq 9 is constant. Fick's law defines the isothermal diffusion coefficient, D:

$$(J_{\mathrm{h}}^{\mathrm{r}})_{\nabla T=0} = -D\frac{c}{x_{\mathrm{l}}}\nabla x_{\mathrm{h}} \tag{10}$$

where c is the total molar concentration of the mixture. We shall also say that Fick's law applies when the ratio Dc/x_l is constant. The D as defined here is exactly the same as the D in the molar reference velocity (de Groot and Mazur, 1969). For isothermal systems, we have from eq 4

$$(J_{\mathrm{h}}^{\mathrm{r}})_{\nabla T=0} = -l_{\mathrm{hh}}\frac{\nabla_T\mu_{\mathrm{h}}}{T} \tag{11}$$

The isothermal diffusion coefficient, D, is related to the phenomenological coefficient, l_{hh}, by

$$D = l_{\mathrm{hh}}R\frac{x_{\mathrm{l}}}{cx_{\mathrm{h}}}\left(1 + \frac{\partial \ln f_{\mathrm{h}}}{\partial \ln x_{\mathrm{h}}}\right) \tag{12}$$

where f_h is the activity coefficient of the heavy component, with activities on a mole fraction basis. We note at this point that all the factors except the thermodynamic factor, *i.e.*, the parentheses at the right-hand side of eq 12, are positive. The thermodynamic factor is also normally positive (Taylor and Krishna, 1993), but in extreme cases (like for phase splitting), $\partial \ln f_h/\partial \ln x_h$ may be smaller than −1, with a negative "diffusion coefficient" as the result. We shall see that local conditions near the vapor/liquid interface for a nonideal mixture is one such case.

In the presence of a temperature gradient, the mass transport is described by a combination of eqs 4 and 10:

$$J_{\mathrm{h}}^{\mathrm{r}} = -D\frac{c}{x_{\mathrm{l}}}\left(x_{\mathrm{h}}x_{\mathrm{l}}\alpha_{\mathrm{hl}}\frac{\nabla T}{T} + \nabla x_{\mathrm{h}}\right) \tag{13}$$

where α_{hl} is the thermal diffusion factor defined by

$$\alpha_{\mathrm{hl}} = -\frac{T}{x_{\mathrm{h}}x_{\mathrm{l}}}\left(\frac{\nabla x_{\mathrm{h}}}{\nabla T}\right)_{J_{\mathrm{h}}=J_{\mathrm{l}}=0} \tag{14}$$

We shall use constant mass fluxes, J_h and J_l, in this work. The separation flux, J_h^r, is not constant, however. The total heat flux referring to the wall or the interface, which here is the enthalpy flux, J_H, is related to the measurable heat flux by

$$J_{\mathrm{H}} = J_q + H_{\mathrm{h}}J_{\mathrm{h}} + H_{\mathrm{l}}J_{\mathrm{l}} \tag{15}$$

where H_k is the partial molar enthalpy of component k. Conservation of energy means in the stationary state that the enthalpy flux is constant throughout the system.

When we eliminate the chemical force $\nabla_T\mu_h/T$ from eq 3 by application of (4), the entropy production rate

can be written as

$$\theta = \lambda\left(\frac{\nabla T}{T}\right)^2 - \frac{l_{hq}}{l_{hh}}J_h^r\frac{\nabla T}{T^2} + \frac{l_{qh}}{l_{hh}}J_h^r\frac{\nabla T}{T^2} + \frac{(J_h^r)^2}{l_{hh}} \quad (16)$$

Two of the terms in eq 16 cancel because $l_{hq} = l_{qh}$. The total entropy production rate in the vapor, liquid, and interface per unit interfacial area is therefore

$$\Theta = \int_g^l \left[\lambda\left(\frac{\nabla T}{T}\right)^2 + \frac{(J_h^r)^2}{l_{hh}}\right] dx \quad (17)$$

where the local entropy production is integrated from across the system, from the bulk gas (g) to the bulk liquid (l). The entropy production is positive, in agreement with the second law of thermodynamics. Equation 17 expresses that the energy needed in excess of ΔG (cf. eq 5) increases with increasing superheating of the vapor (∇T) and with increasing separation flux, J_h^r. It is reduced by a high mass-transfer coefficient l_{hh}, and also by a high coupling coefficient, l_{hq}, or heat of transfer, q^*, since in eq 8 the term $l_{hq}l_{qh}/l_{hh}$ reduces the heat conductivity and thereby the entropy production rate.

Equation 17 will be used for a discussion of relative contributions to the entropy production rate. It differs from eq 1 in the way that it gives a clear separation between the dissipation by pure heat conduction and by pure mass transfer. In eq 1, the heat flux in the first term also contains an effect from the mass flux and vice versa for the mass flux in the second term.

It is a problem that the transport coefficients for heat and mass transfer generally are not known. Introduction of average transport coefficients can simplify the situation. When we consider serial transports, it is appropriate to consider the average *resistance* to the flux. Since J_h^r is constant across the system, the average transport coefficient enters as the coefficient of the second term of eq 17.

$$\frac{1}{l_{ij}} = \frac{1}{L}\int_g^l \frac{dx}{l_{ij}(x)} \quad (18)$$

where L is the length of the path. The application of eq 18 facilitates numerical analyses of eq 17. We shall discuss briefly the possibility of finding such average coefficients.

Molecular Dynamics Simulations of the Coupled Transport of Heat and Mass

The basis for our NEMD simulations is described elsewhere (Ikeshoji and Hafskjold, 1994; Hafskjold et al., 1993; Hafskjold and Kjelstrup Ratkje, 1995), and we shall only briefly describe the method here. The main purpose of the simulations is to study how the different variables and derived properties vary across the interface between liquid and vapor. In order to obtain a sufficient statistical accuracy of computed results, in particular for the vapor phase, we will have to use temperature and concentration gradients in the simulations which exceed the real gradients in a column by several orders of magnitude. Still we shall see that useful conclusions can be obtained. The size of the simulation box is some 35 molecular diameters. This is a range which barely extends the interface. It can be regarded to cover the laminar dissipative films in the bulk vapor and liquid phases, which are described by eqs 2 and 3. Our results must be understood within these contexts.

Simulation Method. The MD cell contained 2048 particles, 1024 of each type. The cell was noncubic with aspect ratios $L_x/L_y = L_x/L_z = 8$ (L_q is the length of the cell in the q direction), and it had normal periodic boundary conditions.

The coupled heat and mass transport was generated as follows: The cell was divided into 64 layers of equal thickness perpendicular to the x axis. To generate a heat flux, layers 1 and 64 (counting from one end of the box) were thermostated to a high temperature T_H, and layers 32 and 33 (in the center of the box) were thermostated to a low temperature T_L. In this way, there is a heat source at each end of the box and a heat sink in the center. The high-temperature and low-temperature regions will be referred to as regions H and L, respectively. This gave a symmetry plane in the center of the cell, consistent with periodic boundary conditions. Periodic boundary conditions are used in these simulations in order to obtain sufficient accuracy in the simulation of one liquid/vapor interface. In addition to giving a heat flux from the warm ends to the cold center of the cell, the temperature profile also generated a liquid region in the center with one vapor region at each side. A snapshot of the configuration is shown in Figure 1, where components h and l are represented by black and white circles, respectively. The liquid phase in the center of the cell with vapor at each side is clearly seen.

Mass diffusion was generated by particle swapping from type l to type h in region H and simultaneously from type h to type l in region L. This gave a surplus of type h particles in region H and of type l in region L, with a consequent diffusive mass flux in between.

Finally, a mass flux simulating a net transport from the vapor to the liquid was generated by moving a randomly chosen particle of type h from region L to region H, such that the particle maintained its y and z coordinates, but the x coordinate was shifted by a value $L_x/2$. The particle insertion into layer H was made with a certain probability given by the Boltzmann factor in order to avoid large perturbations to the energy of the system.

Simulation Conditions. The system was a binary mixture of Lennard-Jones/spline particles (Holian and Evans, 1983). Twelve cases were studied as specified in Table 1. In all cases, the Lennard-Jones potential parameters were equal ($\sigma_{hh} = \sigma_{hl} = \sigma_{lh}$), while the mass ratios m_l/m_h were 0.1 and 1 and the parameter ratio $\epsilon_{ll}/\epsilon_{hh}$ was 1.0 or 0.8 (see Table 1). These sets of parameters mean that we are dealing with an ideal isotope mixture in runs 2−7 with $m_l/m_h = 0.1$ and $\epsilon_{ll}/\epsilon_{hh} = 1.0$. This mixture has zero enthalpy of mixing. Nonideality is introduced in runs 8−12 by using $m_l/m_h = 1$ and $\epsilon_{ll}/\epsilon_{hh} = 0.8$. The nonideal mixture has a nonzero enthalpy of mixing and, therefore, an activity coefficient different from unity.

We used $T_H^* = 1.0$, $T_L^* = 0.7$, and the overall number density $n^* = N\sigma_{hh}3/V = 0.4$ in all cases. The reduced temperature is defined as $T^* = k_BT/\epsilon_{hh}$ where k_B is Boltzmann's constant. The phase diagram of this system is to some extent known (Halseid, 1993), and we chose the overall temperature and density in such a way that we got about equal volumes of vapor and liquid in the cell.

Calculation conditions and some results from the NEMD simulations are reported in Table 1. All quanti-

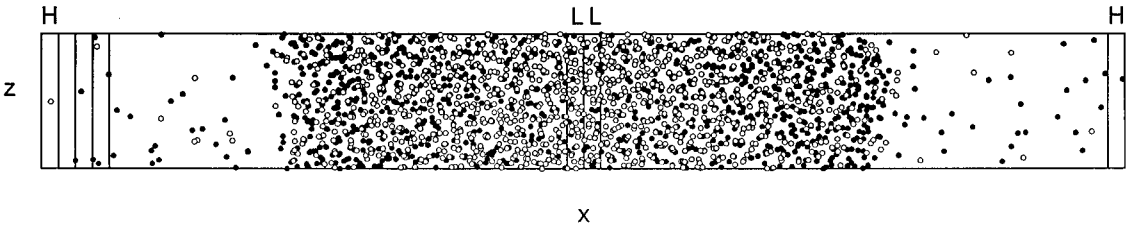

Figure 1. Snapshot of the isotope mixture used in the molecular dynamics simulation. The heavy component is represented by black circles, the light component by white circles. In Ar units, the system has a temperature gradient of approximately -4×10^9 K m^{-1} in the gas and approximately -10^8 K m^{-1} in the liquid. The mole fraction gradient is approximately 10^7 m^{-1} (case 4, Table 1).

Table 1. Simulation Conditions and Results for Enthalpy and Mass Fluxes[a]

comment	case	m_l/m_h	$\epsilon_{ll}/\epsilon_{hh}$	z_h	$10^3 J_H^*$	$10^3 J_h^* \pm 10$	$10^3 J_l^* \pm 10$
pure heat conduction	1	N/A	N/A	1.0	1.64 ± 0.06	N/A	N/A
equimolar overflow distillation	2	1.0	1.0	0.5	1.25 ± 0.05	0.31	−0.31
thermal diffusion	3	0.1	1.0	0.5	2.3 ± 0.2	0	0
equimolar overflow distillation	4	0.1	1.0	0.5	2.2 ± 0.2	0.34	−0.34
equimolar overflow distillation	5	0.1	1.0	0.5	1.8 ± 0.2	1.54	−1.54
distillation	6	0.1	1.0	0.5	2.4 ± 0.2	0.95	−0.59
distillation	7	0.1	1.0	0.5	6.1 ± 0.2	4.06	−1.45
thermal diffusion	8	1.0	0.8	0.8	3.31 ± 0.05	0	0
equimolar overflow distillation	9	1.0	0.8	0.8	2.60 ± 0.06	0.41	−0.41
equimolar overflow distillation	10	1.0	0.8	0.8	2.52 ± 0.08	0.87	−0.87
distillation	11	1.0	0.8	0.8	3.34 ± 0.06	0.66	−0.41
distillation	12	1.0	0.8	0.8	7.16 ± 0.07	3.12	−0.73

[a] Component mass ratio is m_l/m_h, Lennard-Jones/spline potential parameters that vary are $\epsilon_{ll}/\epsilon_{hh}$ ($=\epsilon_{lh}/\epsilon_{hh}$), z_h is the average mole fraction of h in the mixture, J_H^* is the reduced enthalpy flux, and J_h^* and J_l^* are reduced component fluxes. N/A means not applicable.

ties are given in reduced Lennard-Jones units, i.e., reduced enthalpy flux, $J_H^* = J_H(\sigma_{hh}^3/\epsilon_{hh})(m_h/\epsilon_{hh})^{1/2}$, and reduced molar flux, $J_i^* = J_i(\sigma_{hh}3M_h/m_h)(m_h/\epsilon_{hh})^{1/2}$, where M_h is the molar mass of h. The details of the calculation of the temperature (from the equipartition principle), the fluxes, and the forces were given before (Hafskjold et al., 1993). The entropy production rate was calculated from eq 1.

Case 1 of the NEMD simulations is a case of pure heat conduction for the single component h. The heat flux, J_q, is constant across the interface. Cases 2−7 represent ideal mixtures, while cases 8−12 are for nonideal mixtures; see Table 1.

In cases 2, 4, 5, 9, and 10, we used $J_l = -J_h$ to study the assumption of constant molal overflow. These cases have contributions to J_q from both heat and mass transfer. For the ideal mixture, the heat of vaporization of component l exactly cancels the heat of condensation of component h.

Cases 3 and 8 represent pure heat conduction in ideal (case 3) or nonideal (case 8) mixtures. Cases 6, 7, 11, and 12 represent combinations of intermolecular diffusion, condensation, and evaporation. These are the cases that model distillation in general, as component h condensates and l evaporates.

Results and Discussion

The results for the density, composition, and temperature as a function of distance x are given in Figures 2, 3, and 4. Figure 3 gives the separation of mass for the temperature gradients of Figure 4. The heat flux and the relative mass flux are given in Figures 5 and 6, while the entropy production rate is shown in Figures 7 and 8 for cases 1−8 and for a homogeneous binary mixture, respectively. All results are given in dimensionless variables is these figures.

Numerical Results for an Ar-like Isotope Mixture. The results reported in this work can be used with any mixture for which the molecular diameter, σ, the mass of the heavy component, m_h, and the Lennard-Jones potential energy depth, ϵ/k_B, are known. For the sake of getting some numerical insight, we shall use an ideal mixture with mass ratio $m_l/m_h = 0.1$. For Ar-like particles, we then have the diameter 3.405 Å, the mass 6.64×10^{-26} kg, and $\epsilon/k_B = 120$ K. (The resulting separation has no practical interest.) The average temperature gradients over the system are then enormous, -4×10^9 K m^{-1} in the vapor and -10^8 K m^{-1} in the liquid. These gradients are very large compared to gradients one can achieve in the laboratory. We have studied earlier such gradients and established by NEMD (Hafskjold and Kjelstrup Ratkje, 1995) that the basic assumption of nonequilibrium thermodynamics, that of local equilibrium, is still valid.

We get an order-of-magnitude estimate for the dissipated energy by separating an equimolar mixture of h and l in $\Delta t = 1$ s, for $A = 1$ m^2 transfer area by integrating the equation, using estimates of the average values for T and θ:

$$\Theta \approx T\theta A \Delta x \Delta t \tag{19}$$

Here Δx is the distance needed to achieve pure components in the actual composition gradient. We choose the reduced variables $m^* = 1$, $T^* = 1$, $n^* = 0.4$, $J_h^* = 10^{-3}$, $J_H^* = 10^{-3}$, and $\theta^* = 10^{-4}$, which correspond roughly to case 5. Using Ar as an example, we then get $T = 120$ K, $n = 16\,800$ mol m^{-3}, $J_h = 6650$ mol m^{-2} s^{-1}, $J_H = 6.7 \times 10^6$ J m^{-2} s^{-1}, and $\theta = 1.6 \times 10^{13}$ J K^{-1} m^{-3} s^{-1}. The mole fraction gradient read from Figure 3 for case 5 converted to Ar units gives that $\Delta x = 1.8 \times 10^{-8}$ m is needed for full separation. This gives the total dissipated energy equal to 35×10^6 J (for 6650 mol). For comparison, the Gibbs energy of demixing the equimolar mixture into pure components under the same conditions is 9×10^6 J. The total work needed to perform the separation is the sum of the two, 44×10^6 J, leading to a second law efficiency for the separation of 20% (eq 5). This efficiency is not realistic for several reasons. Firstly, it assumes that separation takes place in one step. Secondly, it assumes that products are

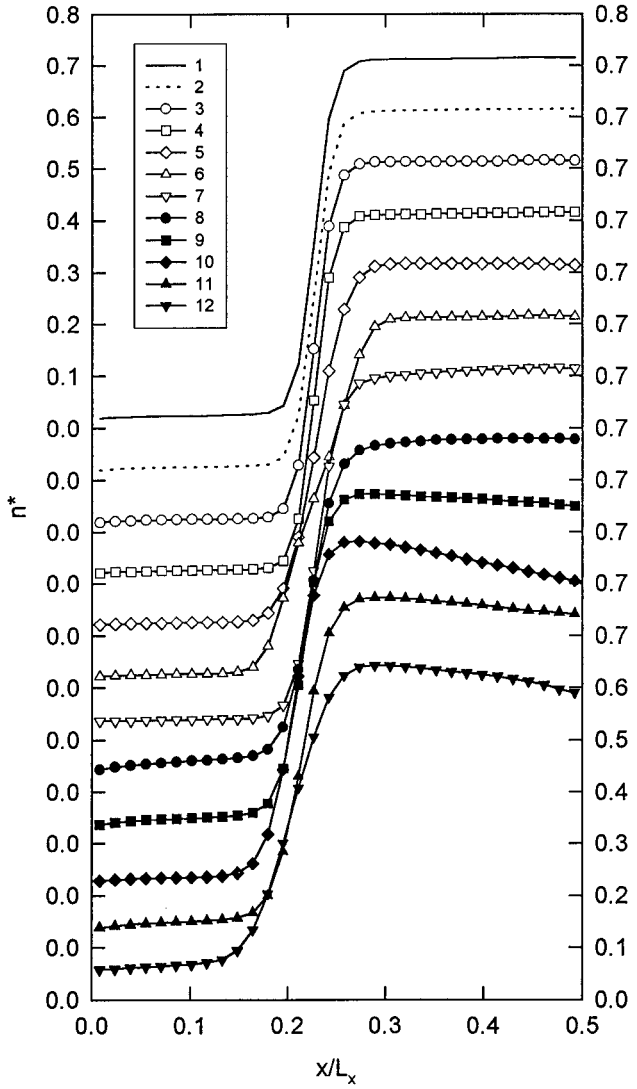

Figure 2. Density profiles across the vapor/liquid interface for the systems specified in Table 1.

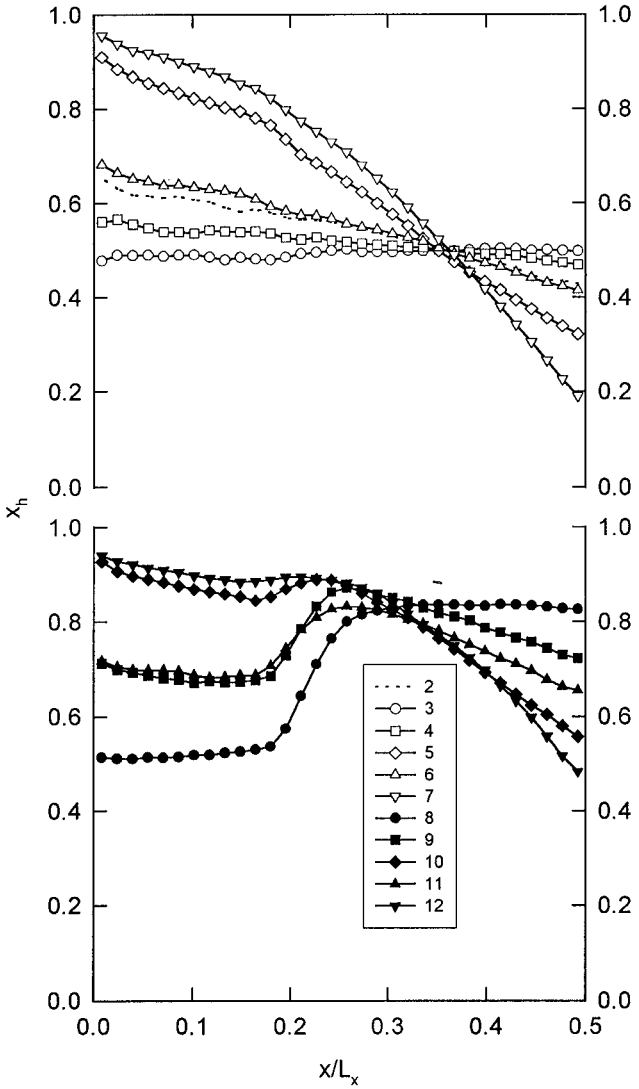

Figure 3. Mole fraction profiles across the vapor/liquid interface for the systems specified in Table 1.

completely pure. The fluxes used in this example are much larger than the experimentally realistic ones. Still, the calculation serves the purpose of showing *how* the entropy production rate and efficiencies can be obtained, and it shows that the presented numbers relate to each other in a reasonable way. According to this, the results of Figures 2−8 can be used to discuss relative variations representative of real distillation problems. Smaller gradients lead to smaller fluxes, but relative variations will remain the same when transport coefficients are constant.

Density, Composition, and Temperature Variations across the Interface. Consider first the number density profiles and the corresponding mole fraction profiles for the heavy component in Figures 2 and 3, respectively.

Figure 2 shows an interface region of thickness 5−8 molecular diameters. This distance covers the range where the number density varies between bulk gas and bulk liquid values. We see that the position of the interface, as measured by the inflection point of the density profile, does not vary significantly. On the scale used in the plot, the gas density of the isotope mixture is small and independent of the mole fraction, x_h, in the gas. The gas density of the nonideal mixture is larger, because component l is now more volatile ($\epsilon_{ll} < \epsilon_{hh}$) and it varies with x_h. The vapor volume of the nonideal mixture is slightly smaller than that of the ideal mixture for a given average molar fraction of l, because of this. Volume changes in the liquid and vapor streams have an impact on the operating line.

While the ideal mixtures in all cases have a monotonous variation of x_h across the interface (see, e.g., cases 4−7, Figure 3), the nonideal mixtures have a *local maximum* in x_h at the interface (see, e.g., cases 9 and 11). The chemical potential gradient is related to the mole fraction gradient simply by $\nabla_T \mu_h = RT\nabla \ln x_h$ for the ideal isotope mixture. The variation in the thermodynamic force $\nabla_T \mu_h$ is therefore continuous across the interface. If the same applies to the nonideal mixtures, the additional term $RT\nabla \ln f_h$ varies in a nonmonotonous way; *i.e.*, the activity coefficient depends strongly on the position across the interface.

The approximately linear mole fraction profiles in the liquid phase as well as in the gas phase in cases 3, 4, and 6 of the ideal mixtures show that the product Dc/x_l is approximately constant across the interface. This does *not* lend support to the correlation for D introduced by Sigmund (1976), in which Dc, not Dc/x_l, is assumed to be constant over a wide density range. The Sigmund correlation was *not* also a good approximation for nonideal mixtures, according to experimental results for the methane/*n*-decane mixture (Dysthe et al., 1995). For the ideal mixtures, cases 3, 4, and 6, Fick's law can be

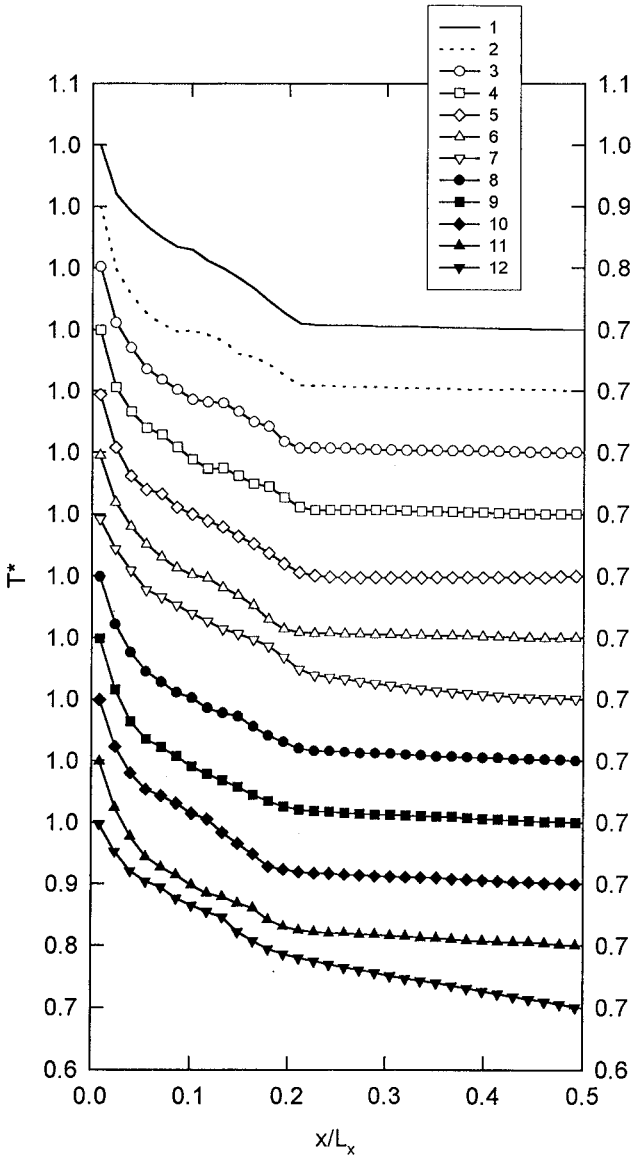

Figure 4. Temperature profiles across the vapor/liquid interface in the stationary states given in Table 1.

used with constant Dc/x_l also across the interface. This cannot be done for cases 5 and 7, where the diffusive fluxes are larger and Dc/x_l jumps at the surface. The difference between cases 4 and 5 is noteworthy since these cases model similar situations: equimolar diffusion. It is the difference in molar flux that gives the difference in mole fraction profiles between cases 4 and 5, as the heat flux is very similar in the two cases (see Table 1).

The nonideal mixtures have a region near the interface where diffusion occurs *against* the composition gradient. The consequence is that the mutual diffusion coefficient, as defined locally by Fick's law, is negative in this region, cf. eq 10. The transport is, however, *along with* the chemical potential gradient. The transport is also along the temperature gradient. The process is therefore not in disagreement with the second law of thermodynamics. The importance of using forces for the transports given by nonequilibrium thermodynamics is emphasized by this finding.

We conclude that the product Dc/x_l in Fick's law is constant in bulk mixtures of ideal liquids and gases. At the interface, there may be a jump in this variable. The product may be taken as constant for bulk nonideal gas and liquid mixtures only with great care. Fick's law fails in the surface region of the these mixtures.

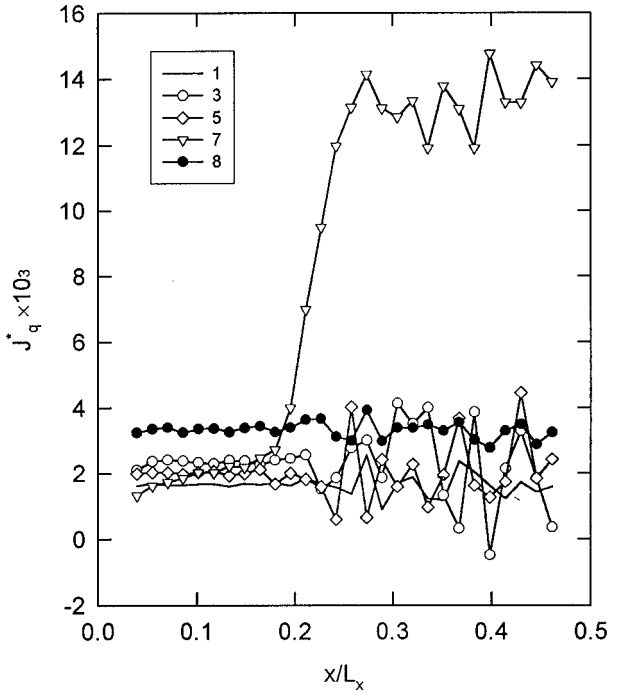

Figure 5. Variation in the heat flux across the interface for some selected ideal (white symbols) and nonideal (black symbols) mixtures.

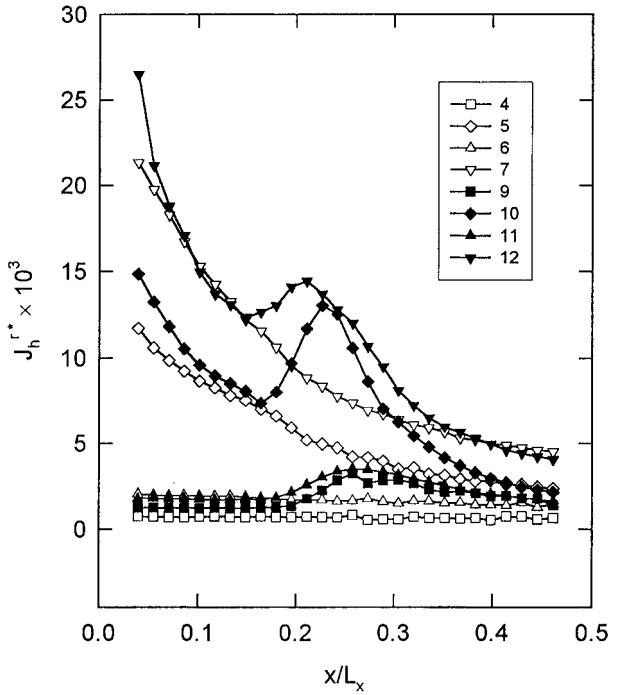

Figure 6. Relative molar flux across the interface for some selected ideal (white symbols) and nonideal (black symbols) mixtures.

The temperature profiles for all cases studied are shown in Figure 4. All cases have a linear temperature profile in the liquid phase, which means that the heat conductivity of Fourier's law is constant in this phase. The relatively small temperature gradients in the liquid phase mean that the heat conductivity is larger for this phase than for the vapor. Cases 1, 3, and 8 were used to compute the thermal conductivity. A significant increase from gas to liquid and a smooth variation

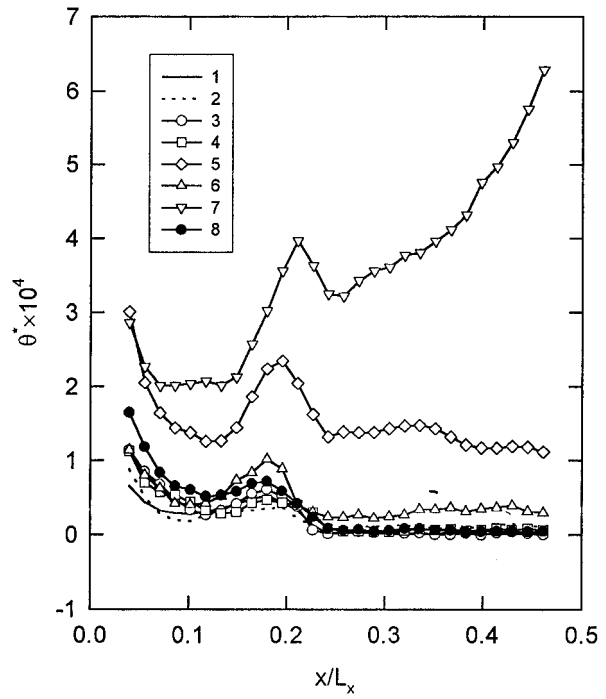

Figure 7. Entropy production rate for heat and mass transport across an interface with ideal (white symbols) and nonideal (black symbols) mixtures.

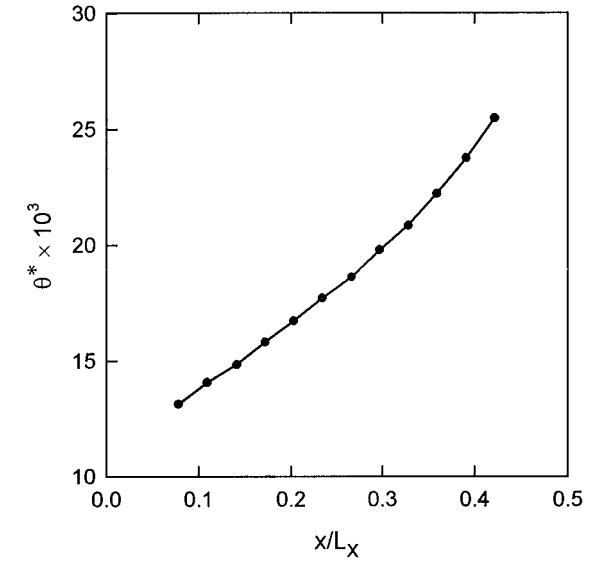

Figure 8. Entropy production rate for heat and mass transport in an ideal homogeneous mixture.

across the interface was found (not shown here). Fourier's law can then be applied locally only when the position dependency of the heat conductivity is known.

The most interesting feature of the stationary-state temperature profile in the gas phase and through the interface is its nonlinearity near the interface. The nonlinear part near $x/L_x = 0$ is a "wall" effect of the H layers due to the thermostat and low density, but the shoulder that shows in most profiles is due to properties of the gas−liquid system. It should be noted that even the simple cases of heat conduction only (cases 1, 3, and 8) show the shoulder in the temperature profile. The position of the shoulder is clearly on the gas side of the interface. An independent simulation of a single-phase vapor mixture subject to the same temperature difference did not give this shoulder. We conclude that the shoulder is a consequence of heat effects at the liquid/vapor interface. This has support in kinetic theory (Ytrehus and Østmo, 1996) and molecular dynamics simulations (Yasuoka et al., 1995). Different kinetic energies are then associated with the condensing and evaporating molecules, and these energies must have an impact on the steady-state distribution of mass in the temperature gradient (the Soret equilibrium), cases 3 and 8 (Hafskjold et al., 1993).

We know that the Soret effect can be neglected in the vapor phase and gives a 10% contribution from the first term of eq 13 in the liquid phase (Kincaid et al., 1992; Kincaid and Hafskjold, 1994). At the surface, the Soret effect is as yet unknown. We have seen that the presence of an interface has an impact on the temperature profile in the gas phase. It therefore appears that a bigger value can be expected at the interface than in the bulk phases. We predict a big value from eq 24 below.

Heat Flux across the Phase Boundary. The heat fluxes for selected cases are shown in Figure 5. The general picture is that the heat flux is close to constant in the bulk phases, but in cases with a source term at the interface (the heat of condensation), it changes sharply at the interface, i.e. the coupling coefficients of eqs 3 and 4 are significant. This is illustrated by case 7, in which there is a net condensation of vapor ($|J_h| > |J_l|$). In cases 1, 3, and 8, J_q is constant because $J_l = J_h = 0$. In case 5, J_q is constant because $J_l = -J_h$ and the two components have the same heat of vaporization.

Equation 15 explains why the measurable heat flux, J_q, is generally not constant throughout the system. Generally, the last terms contribute. Neglecting the contributions from the heat of mixing, we may rewrite the heat flux of eq 15:

$$J_q^l = J_q^v + \Delta_{vap}H_l J_l + \Delta_{vap}H_h J_h \qquad (20)$$

where superscripts l and v represent liquid and vapor, respectively, and Δ_{vap} represents a change upon vaporization. Depending on the relative magnitude of the fluxes, the first or the last two terms on the right-hand side of eq 20 may be small compared to the other terms. For small temperature gradients, it may be useful to assume that the heat flux in the liquid phase is given by the net heat effect of condensation and evaporation, i.e., the last two terms of eq 20. This means that we can write

$$J_q^l \approx \Delta_{vap}H_l J_l + \Delta_{vap}H_h J_h \qquad (21)$$

These terms will sum to a constant when the mass fluxes are constant. Constant mass fluxes were used throughout these simulations, meaning that the approximation (21) is valid only for case 7 in Figure 5. In the other cases of this figure, we have $J_q^l = J_q^v$.

The pure heat conductance term (the first term on the right-hand side of eq 20 since the thermal diffusion factor is small) is of the order $2-3 \times 10^{-3}$ in Lennard-Jones units as taken from Figure 5. Although the scatter of the data is higher in the liquid than in the vapor, J_q^l is of the same order in all the cases shown except case 7, where it is approximately 13×10^{-3}. In case 7, there is a net mass flux from the vapor to the liquid, which means that there is a significant heat source due to condensation at the interface (see eqs 7 and 20). Even though there is also a diffusive mass flux in case 5, it does not give a heat source since the heat of condensation of component h exactly cancels the heat

of vaporization of component l in the isotope mixture. Cases 1, 3, and 8 are cases of pure heat conduction in systems without net mass flux.

The approximation (21) is not generally true for condensation or distillation. Equimolar diffusion of the components in ideal mixtures gives no heat sink or source at the interface, and then the terms of eq 21 cancel, and vice versa, equimolar diffusion need not be maintained when the enthalpies of vaporization are different as in case 9 or 10. This result is in agreement with the conclusion reached long ago by Krishna (1977) from analysis of multicomponent distillation.

Nonequilibrium thermodynamics gives, for these reasons, a more accurate description of distillation than the equilibrium stage model. From knowledge of the heat of transfer, one may calculate the impact of the mass flux on the heat flux in eq 7. This will further determine the mass or volume of the bulk streams in a distillation column, the operating line, and the number of theoretical stages.

Relative Mass Flux across the Interface. The relative mass flux, J_h^r, is shown in Figure 6. We see a systematic difference between the fluxes for ideal and nonideal mixtures. The ideal mixtures, cases 4−6, are not associated with a large change in composition across the interface, and J_h^r is monotonous. The nonideal mixtures, cases 9−12, show an interesting feature: There are extremal values for J_h^r at the interface.

A minimum in J_h^r represents a tendency to collective motion of the two components, whereas a maximum in J_h^r indicates a strong tendency for separation at the interface, cf. eq 6, in accordance with $\partial \ln f_h/\partial \ln x_h$ being negative in eq 12. When the thermodynamic driving force, $\nabla_T \mu_h/T$, is monotonous across the interface, the phenomenological coefficient, l_{hh}, has a a maximum at the interface and a minimum just outside (on the vapor side). Physically, this means that the rate-limiting step for mass transfer is in the vapor. The explanation for the maximum at the interface is that the equilibrium compositions favor a higher concentration of h in the liquid than in the vapor and vice versa for component l (see Figure 2). Since fluxes J_h and J_l are constant across the interface, the maximum in J_h^r is a direct consequence of the mole fraction ratio x_h/x_l in eq 2. Although there is probably no anomaly in the thermodynamic driving force, the equilibrium compositions are such that separation is enhanced at the interface. The minimum in J_h^r is more subtle, although it may simply be a consequence of the maximum discussed above, superimposed on the sloping curves we also see for the ideal mixtures. The apparent collective motion may, however, also be a separate phenomenon near the interface and, like the shoulder in the temperature profile shown in Figure 4, be related to the escape/capture process between the vapor and the liquid.

The relative mass fluxes for cases 2, 4, and 6 show a smaller change in J_h^r at the interface. The fluxes are also relatively small. Considering the large gradients that we apply in the simulation, we may expect a nearly constant value in practical situations for such ideal mixtures.

Heat of Transfer. One procedure to find the heat of transfer can be obtained by combining eqs 7 and 20, which gives for the liquid phase

$$q^* = \frac{J_q^v + \Delta_{vap}H_l J_l + \Delta_{vap}H_h J_h + (\lambda \nabla T)^l}{J_h^r} \quad (22)$$

where superscripts v and l represent vapor and liquid, respectively. For equimolar overflow, $J_l = -J_h$, this expression reduces to

$$q^* = \frac{J_q^v + (\lambda \nabla T)^l}{J_h^r} + (\Delta_{vap}H_h - \Delta_{vap}H_l)\frac{J_h}{J_h^r} \quad (23)$$

We found from Figure 5 that the measurable heat flux for the *ideal mixtures* was rather independent of the mass fluxes in the gas phase for equimolar flow and constant across the interface. This implies that $J_q^v \approx -\lambda \nabla T$, and the numerator in the first term on the right-hand side of eq 23 vanishes. In such cases, the model

$$q^* \approx (\Delta_{vap}H_h - \Delta_{vap}H_l)\frac{J_h}{J_h^r} \approx \text{constant}(\Delta_{vap}H_h - \Delta_{vap}H_l) \quad (24)$$

should be reasonably good. For ideal mixtures with $\Delta_{vap}H_h \approx \Delta_{vap}H_l$, we than see that q^* vanishes at the interface. This explains why the interface has such a small impact on the separation of isotopes, cf. upper part of Figure 3. The heat of transfer can always be expected to be significant at the interface for nonideal mixture distillation, as exemplified by cases 9, 10, and 6.

The value of J_h^r differs from stage to stage in a distillation column, depending on the driving forces for separation at the stage in question. This means that q^* probably varies across the column. The heat of transfer may be positive or negative depending on the relative magnitude of the two heats of vaporization in eq 22. This has an impact on the action of the forces of eqs 3 and 4. The forces may enhance or counteract each other, depending on the sign of q^*. A positive thermal force reduces J_h^r when q^* is negative. A positive value for the heat of transfer is beneficial when a large value for J_{hr} is wanted.

Entropy Production Rate. The local entropy production rate from the thermal flux and force and the mass separation flux and force was calculated according to eq 1 and shown in Figure 7.

The first conclusion to be drawn from this is that the entropy production rate of the surface may be significant compared to the entropy production rates in layers of similar thickness in the adjoining bulk phases. It is only when the mass fluxes are at the largest (case 7) that the entropy production rate in the liquid becomes *much* larger than that of the surface. Otherwise, the values are comparable in magnitude. We expect that this will hold also for smaller (real) gradients. All parts of the entropy production rate therefore play a role in the excess energy needed in terms of ΔG in eq 5. This fits with practical experience. It is hard to make a clear-cut assignment of the phase which is rate limiting for column performance.

The contribution from the thermal flux and force to the entropy production rate is generally smaller than the contribution from the chemical flux and force, and it is negligible in the liquid. However, the peak near the interface is dominated by the thermal contribution (not shown) and can account for as much as one-third of the total entropy production rate in the vapor (Haf-

skjold and Kjelstrup Ratkje, 1996). The entropy production rate is of the same order of magnitude in the liquid and vapor. These results do not support the assumptions made by Kjelstrup Ratkje et al. (1995) in their estimation of the entropy production rate, viz. neglecting the thermal contribution to the entropy production and the entropy production in the liquid phase. We see that NEMD can be used to give the local value of the entropy production rate.

Comparison of eqs 1 and 17 gives that, if $l_{hq} = l_{qh} > 0$ (usually the case), it is better to neglect the "thermal contribution" to the entropy production rate in eq 17 than in eq 1. In eq 17, the two terms proportional to the coupling terms in eq 16 cancel. The finite value of the coupling term reduces the thermal contribution (cf. eq 16) and increases the contribution from the mass flux. For the same reason, it is better to neglect the contribution from the mass flux in eq 1 than in eq 17. The two forms therefore serve different purposes.

The striking feature of Figure 7 is that all simulations performed even for the one-component system show a maximum in the entropy production rate slightly at the vapor side of the interface. The maxima are larger for cases which have a nonnegligible q^*.

By contrast, the entropy production rate in a homogeneous ideal two-component mixture shows a monotonous increase from the hot to the cold side (Figure 8). The entropy production rate is *not* uniformly distributed in the stationary state, neither in the one-component system nor in the two-component system.

The results also show that forces are generally not constant across the interface. The *concentration* gradients in the liquid and gas ideal mixtures are constant (Figure 3). The *temperature* gradients are constant only in the liquid phase (Figure 4) (for both ideal and nonideal mixtures). Consequently, the definition of an average diffusion coefficient for transport across the interface (eq 18) is easy for ideal mixtures; otherwise, the definition is nontrivial in the sense that the integrand in eq 18 may change abruptly across the interface. More work is needed to find such average coefficients.

We have previously studied molecular mechanisms of transport of heat and mass in one-phase systems in the stationary state (Hafskjold et al., 1993; Hafskjold and Kjelstrup Ratkje, 1995). The heat was most effectively conducted in this state by a distribution of the components which gave a constant-concentration gradient in a constant-temperature gradient. When a liquid−gas transition is involved, it is clear from Figure 3 that effective heat transfer does not imply such a simple distribution. We intend to examine how the system responds most effectively to given boundary conditions on a molecular level in a future work.

Liquid/Vapor Surface. This study has shown that the surface has special transport properties and that it is necessary to use nonequilibrium thermodynamics in the description of transport in this region. A larger portion of the energy dissipated in the system is dissipated at the surface. (This part of the dissipation is probably unavoidable in the distillation column.)

The special properties of the surface region indicate that the surface can be regarded as a separate system in the thermodynamic sense, a topic we shall elaborate on in a future article. It is possible to compute all variables of Figures 2−8 in a well-defined manner also in the surface region. The length scale for our investigation is a molecular one (in nanometer), not a macroscopic scale (in micrometers). A formulation of the transport problem on a micrometer scale can be obtained by integration over the surface variables; see Bedeaux et al. (1992). Albano et al. (1979) showed that the dynamic behavior of the interfacial densities can be given in terms of interfacial fluxes and extrapolated bulk densities and fluxes alone. The description is equivalent to a description which uses densities and fluxes which are singular at the surface. The intriguing shoulder of the temperature profile (Figure 4) is an indication that singularities may occur in such a macroscopic description.

Applications to Distillation. The present work is an attempt to encourage work on nonequilibrium thermodynamic modeling of distillation. We have shown how forces and fluxes during distillation of binary mixtures can be defined locally and how they can be included into an efficiency calculation of the process.

Severe gradients have been applied in the study, but this means that the general conclusions can be transferred with certainty to less severe situations. Nonequilibrium molecular dynamics simulation yields values for transport coefficients under conditions that are hardly accessible in practice. The fact that transport data for the complex transport equations (3 and 4) are available through computer simulations may facilitate the application of nonequilibrium modeling of distillation columns. The coefficients obtainable from the present data and their molecular interpretation will be discussed in a further work.

In our simulation technique, we set the condition of equimolar overflow in the computer experiment and investigated its consequences (cases 2, 4, 5, 9, and 10). In the real case, the situation is different: The heat supply to the column is controlled (adiabatic column), and separation follows. When we see a net heat effect at the surface in our simulations, we know that the last term of eq 7 plays a role. This is compatible with a bending operating line. The sign of the heat of transfer will relate to the curvature of the operating line. A positive value for q^* means that the heavy component has a higher flux than the light component (cf. eq 13). The volume of the vapor phase may be reduced, and the operating line in the rectifying section, say, will increase its slope. It should be possible to find a revised number of theoretical stages needed from this information.

We have found that average phenomenological coefficients (eq 18) can be calculated by integrating across each of the phases in the ideal system. The assumption of a negligible contribution to the entropy production rate from the liquid phase (Kjelstrup Ratkje et al., 1995) was not substantiated from these data, however. The present results mean that the entropy production rate of distillation may depend on the transport properties of the surface. This means that it will be important to find transport coefficients for the surface.

Conclusions and Perspectives

The present work is an attempt to get direct information on the relationship between the molecular and macroscopic heat- and mass-transfer properties at the gas/liquid interface. We have seen that the ordinary Fick's and Fourier's laws can be used for the liquid and gas separately. As soon as the mixture is not ideal, the thermodynamic equations of transport are needed, and the properties of the liquid−vapor interface have to be taken into account.

On a molecular (nanometer) scale, the intensive variables of the system are smooth functions across the

interface. There are, however, indications of an anomaly in the temperature profile (a shoulder). Nonequilibrium thermodynamics for surfaces may therefore give a discontinuity in the temperature at a macroscopic scale. More work is needed to establish the boundary conditions for integrations across the surface in this case.

The entropy production rate has a peak near the interface in all the cases we have studied in this work. This peak stems from the shoulder in the temperature profile. In the cases studied, the entropy production is of the same order of magnitude in the gas and liquid. The thermal and mass-transfer contributions to the entropy production are also comparable in magnitude.

We have indicated how the equations of transport given by nonequilibrium thermodynamics can be used to analyze the efficiency of column elements and calculate operating lines. The burden of getting transport coefficients can probably also be eased by application of nonequilibrium molecular dynamics simulation techniques.

Acknowledgment

B.H. thanks the Agency of Industrial Science and Technology (AIST) and TRU at the University of Oslo for providing computer resources for this work. B.H. is also grateful to AIST for financial support during his sabbatical stay there.

Literature Cited

Albano, A. M.; Bedeaux,D.; Vlieger, J. On the Description of Interfacial Properties Using Singular Densities and Currents at a Dividing Surface, *Phys. A* **1979**, *99*, 293.

Bedeaux, D.; Hermans, L. J. F.; Ytrehus, T. Slow Evaporation and Condensation. *Phys. A* **1990**, *169*, 263.

Bedeaux, D.; Smit, J. A. M.; Hermans, L. J. F.; Ytrehus, T. Slow Evaporation and Condensation. II. A Dilute Mixture. *Phys. A* **1992**, *182*, 388.

de Groot, S. R.; Mazur, P. *Non-Equilibrium Thermodynamics*; North-Holland: Amsterdam, 1961; Dover: New York, 1985.

Dhole, V. R.; Linnhoff, B. Distillation Column Targets. *Comput. Chem. Eng.* **1993**, *17*, 549.

Dysthe, D. K.; Hafskjold, B.; Breer, J.; Cejka, D. An interferometric technique for measuring interdiffusion at high pressures. *J. Phys. Chem.* **1995**, *99*, 11230.

Førland, K. S.; Førland, T.; Kjelstrup Ratkje, S. *Irreversible Thermodynamics. Theory and Applications*; John Wiley & Sons: Chichester, 1988; 2. Reprinted 1994.

Hafskjold, B.; Ikeshoji, T. Partial specific quantities computed by nonequilibrium molecular dynamics. *Fluid Phase Equilib.* **1995**, *104*, 173.

Hafskjold, B.; Ikeshoji, T. Non-equilibrium molecular dynamics simulation of coupled heat- and mass transport across a liquid/vapor interface. *Molec. Simul.* **1996**, in press.

Hafskjold, B.; Kjelstrup Ratkje, S. Criteria for local equilibrium in a system with transport of heat and mass. *J. Stat. Phys.* **1995**, *78*, 463.

Hafskjold, B.; Kjelstrup Ratkje, S. Molecular Interpretation of couples transport of heat- and mass transport across a vapor/liquid interface. In *ECOS'96 Symposium Proceed*; Alvfors, P., Eidensten, L., Svedberg, G., Yan, J., Eds.; Dept. of Chem. Eng., Royal Insitute of Technology: Stockholm, 1996; p 405.

Hafskjold, B.; Ikeshoji, T.; Kjelstrup Ratkje, S. On the molecular mechanism of thermal diffusion in liquids. *Molec. Phys.* **1993**, *80*, 1389.

Halseid, R. The Critical Point of the Lennard-Jones Spline Fluid, Project Report, Norw. Inst. of Technology, Trondheim, 1993.

Holian, B. L.; Evans, D. J. Shear Viscosities away from the Melting Line: A Comparison of Equilibrium and Nonequilibrium Molecular Dynamics. *J. Chem. Phys.* **1983**, *78*, 5147.

Ikeshoji, T.; Hafskjold, B. Non-equilibrium Molecular Dynamics Calculation of Heat Conduction in Liquid and through Liquid-Gas Interface. *Molec. Phys.* **1994**, *81*, 251.

Kincaid J. M.; Hafskjold, B. Thermal Diffusion Factors for the Lennard-Jones/spline System, *Molec. Phys.* **1994**, *82*, 1099.

Kincaid, J. M.; Li, X.; Hafskjold, B. Nonequilibrium Molecular Dynamics Calculation of the Thermal Diffusion Factor. *Fluid Phase Equilib.* **1992**, *76*, 113.

Kjelstrup Ratkje, S.; Hafskjold, B. Coupled Transports of Heat and Mass. Theory and Applications. In *Entropy and Entropy Generation: Fundamentals and Applications*; Shiner, J., Ed.; Kluwer: Dordrecht, 1996, in press.

Kjelstrup Ratkje, S.; Sauar, E.; Hansen, E. M.; Lien, K. M.; Hafskjold, B. Analysis of Entropy Production Rates for Design of Distillation Columns. *Ind. Eng. Chem. Res.* **1995**, *34*, 3001.

Krishna R. A film model analysis of non-equimolar distillation of multicomponent mixtures. *Chem. Eng. Sci.* **1977**, *32*, 1197.

Linnhof, B.; Townsen, D. W.; Boland, D.; Hewitt, G. F.; Thomas, B. E. A.; Guy, A. R.; Marsland, R. H. User Guide on Process Integration for the Efficient Use of Energy. *The Institution of Chemical Engineers*; Warks, 1982.

Lydersen, A. *Mass Transfer in Engineering Practice*, Wiley: Chichester, 1983.

Prigogine, I. Etude thermodynamique des phenomenes irreversibles. Thesis, Desoer, Liège, 1947.

Sauar, E.; Kjelstrup Ratkje, S.; Lien, K. M. Process optimization by equipartition of forces. Applications to distillation columns. In *ECOS'95 Symp. Proceed*; Gogus, Y. A., Ozturk, A., Tsatsaronis, G., Eds.; Turkish Soc. for Thermal Sciences and Technology, Mechanical Eng. Dept., Ankara and ASME: New York, 1995; Vol. I, p 413.

Sauar, E.; Kjelstrup Ratkje, S.; Lien, K. M. Equipartition of forces—a new principle for process design and optimization. *Ind. Eng. Chem. Res.* **1996**, in press.

Sigmund, P. M. Prediction of molecular diffusion ar reservoir conditions. Part I. measurement and prediction of binary dense gas diffusion coefficients. *J. Can. Petrol. Technol.* **1976**, April—June, 48.

Taylor, R.; Krishna, R. *Multicomponent Mass Transfer*; John Wiley & Sons: New York, 1993.

Taylor, R.; Lucia, A. Modeling and Analysis of Multi-component Separation Processes. *AIChE Symp. Ser.* **1995**, *91* (304), 19.

Tondeur, D.; Kvaalen, E. Equipartition of Entropy Production. An Optimality Criterion for Transfer and Separation Processes. *Ind. Eng. Chem. Res.* **1987**, *26*, 50.

Yasuoka, K.; Matsumoto, M.; Kataoka, Y. Molecular Simulation of Evaporation and Condensation I. Self Condensation and Molecular Exchange. In *ASME/JSME Thermal Engineering Proceed.*; Fletcher, L. S., Aihara, T., Eds.; The American Society of Mechanical Engineers: New York, 1995

Ytrehus, T; Østmo, S. Kinetic Approach to Interphase Processes. *Int. J. Multiphase Flow* **1996**, *22*, 133.

Received for review April 8, 1996
Revised manuscript received August 23, 1996
Accepted August 29, 1996[⊗]

[⊗] Abstract published in *Advance ACS Abstracts*, October 15, 1996.